CWE-8
June 7-11, 2026
London, ON, Canada

Typhoon Wind Effects on Coastal Infrastructures: A Probabilistic Perspective

Genshen Fang [a], Zihang Liu [b], Yue Cheng [c], Jingkai Cai [d], Yaojun Ge [e]

[a] *State Key Lab of Disaster Reduction in Civil Engineering, Tongji University, Shanghai 200092, China, 2222tjfgs@tongji.edu.cn*
[b] *State Key Lab of Disaster Reduction in Civil Engineering, Tongji University, Shanghai 200092, China, 18579100185@163.com*
[c] *State Key Lab of Disaster Reduction in Civil Engineering, Tongji University, Shanghai 200092, China, 851838638@qq.com*
[d] *State Key Lab of Disaster Reduction in Civil Engineering, Tongji University, Shanghai 200092, China, 2410485@tongji.edu.cn*
[e] *State Key Lab of Disaster Reduction in Civil Engineering, Tongji University, Shanghai 200092, China, yaojunge@tongji.edu.cn*

SUMMARY

Typhoon usually causes significant effects on coastal infrastructures, including long-span bridges, large wind turbines, transmission grids etc. Most current design standards rely on deterministic analysis of wind effects, inadequately addressing the variability of TC wind and fail to answer the reliability or failure probability of the structure. This study bridges this gap using stochastic TC simulations to analyze the failure of coastal structures from a probabilistic perspective. The semi-analytical 3D TC wind model, stochastic TC track model and data-driven turbulence parameter model are introduced to generate 10,000-year synthetic TC events and probabilistic wind fields. The wind dataset is applied to a long-span bridge, a wind turbine and a transmission tower to calculate their long-term structural responses. The variation of internal forces or displacements with wind speed at different positions of the structure are obtained. The annual failure probability of the structure is finally analyzed. The insights inform resilient structural designs in typhoon-prone regions, aiming to mitigate risks and economic losses associated with coastal infrastructure operations.

Keywords: *Typhoon, Wind effects, long-span bridge, wind Turbine, Transmission tower*

1. INTRODUCTION

With an expanding span or height, modern infrastructures exhibit increasing flexibility, thereby elevating the susceptibility to wind excitation. This heightened sensitivity underscores the necessity of accurately assessing the wind environment and quantifying its effects on such structures, particularly those repeatedly exposed to extreme wind events such as typhoons, which commonly affect coastal regions of China. Great efforts have been put in estimating the typhoon-induced vibration of flexible structures, which are usually based on deterministic inputs (Hu et al, 2013). Nonetheless, uncertainties in the structural system, boundary conditions, aeroelastic terms, and external loads can all contribute to the scattered wind-induced vibrations. Typhoon winds, as one of the decisive external loads for coastal infrastructure, exhibit strong variability, which has been proved in many measured data thanks to the advances in field observation techniques. The use of the deterministic wind design parameters provided in codes and standards fails to account for the wide range of typhoon wind variability, and is insufficient to reproduce the stochastic nature of the structure response, which can even lead to underestimation of the measured results(Liu et al., 2022, 2023). Motivated by these challenges, this study adopts a probabilistic perspective to investigate typhoon effects on multiple representative infrastructures along the southeastern coast of China.

2. TYPHOON WIND FIELD MODEL

2.1 Semi-analytical 3D Typhoon Wind Field Model

The TC boundary-layer wind field is derived from the momentum conservation equation (Fang et al., 2019, 2021a):

$$\frac{D\mathbf{V}}{Dt} = \frac{\partial \mathbf{V}}{\partial t} + \mathbf{V} \cdot \nabla \mathbf{V} = -\frac{1}{\rho_a}\nabla \mathbf{P} - f \cdot (\mathbf{k} \times \mathbf{V}) + \boldsymbol{g} + \mathbf{F}_d \tag{1}$$

where $\mathbf{V} = [V_r, V_\theta, V_z]$ is the 3D wind velocity, $p$is pressure, and $\mathbf{F}_v$ is the viscous force. The radial–vertical pressure field is parameterized as:

$$P_{rz} = \left\{ P_{cs} + \Delta P_s \cdot exp\left[-\left(\frac{R_{max,s}}{r} \right)^{B_s} \right] \right\} \cdot \left(1 - \frac{gkz}{R_d \theta_v} \right)^{\frac{1}{k}} \tag{2}$$

where p_c is the central pressure, $\Delta p$the pressure deficit, R_m is the radius to maximum wind speed, and B a radial-shape parameter. Above the boundary layer, the gradient wind speed follows:

$$V_g = \frac{V_{T\theta} - fr}{2} + \sqrt{\left(\frac{V_{T\theta} - fr}{2} \right)^2 + \frac{r}{\rho_{ag}} \frac{\partial P_g}{\partial r}} \tag{3}$$

where f is the Coriolis parameter and V_t is the storm translation velocity. These relations allow simulation of height-varying mean wind-speed profiles at any typhoon life-cycle stage.

2.2 Stochastic Typhoon Track Model

The typhoon track model stochastically generates typhoon paths from genesis to lysis while preserving the statistical characteristics of historical observations. The evolution of key parameters-translation speed V_T, heading direction θ_T, relative intensity I_u, radius to maximum wind speed $R_{\max,s}$, and radial pressure-shape parameter B_s, which can be formulated using recursive relationships calibrated from the JMA Best Track dataset (Fang et al., 2021b):

$$\Delta \ln V_T = v_1 + v_2 \ln V_T\,(i) + v_3 \ln V_T\,(i-1) + v_4 \theta_T(i) + \varepsilon_{\Delta \ln V_T} \tag{4}$$

$$\Delta\theta_T = \theta_T(i+1) - \theta_T(i) = h_1 + h_2\theta_T(i) + h_3\theta_T(i-1) + h_4 V_T(i) + \varepsilon_{\Delta\theta_T} \tag{5}$$

$$\begin{aligned} \ln[I(i+1)] = {} & c_1 + c_2 \ln[I(i)] + c_3 \ln[I(i-1)] + c_4 \ln[I(i-2)] \\ & + c_5 T_s(i+1) + c_6[T_s(i+1) - T_s(i)] + \varepsilon_{\ln(I)} \end{aligned} \tag{6}$$

$$\begin{aligned} \ln R_{max,s}(i+1) = {} & r_1 + r_2 \ln R_{max,s}(i) + r_3 \ln R_{max,s}(i-1) \\ & + r_4 \Delta p_0(i+1) + \varepsilon_{\ln R_{max,s}} \end{aligned} \tag{7}$$

$$B_s(i+1) = b_1 + b_2\sqrt{R_{max,s}(i+1)} + b_3 B_s(i) + b_4 B_s(i-1) + \varepsilon_{B_s} \tag{8}$$

where v_j, h_j, r_j, b_j (j = 1 to 4) and c_k (k = 1 to 6) represent model regression coefficients; ε is error terms constructed to represent the discrepancies between the regression model and the actual measured data; I is the relative intensity of typhoon.

2.3 Probabilistic Turbulence Parameter

The typhoon turbulence spectrum follows (Liu et al., 2022):

$$S(\omega) = \frac{\sigma_u^2 A z}{U\left(1 + 1.5A\frac{\omega z}{2\pi U}\right)^{\frac{5}{3}}} \tag{9}$$

where A is a dimensionless spectral parameter, which is modeled as lognormally distributed with both mean and variance correlated with mean wind speed U.

The along-wind turbulence intensity $I_u(z)$ is described by a GEV distribution:

$$F(x) = \frac{1}{\sigma} exp\left[-\left(1 + k \cdot \frac{x-\mu}{\sigma} \right)^{-\frac{1}{k}} \right] \left(1 + k \cdot \frac{x-\mu}{\sigma} \right)^{1-\frac{1}{k}} \tag{10}$$

where the parameter μ and scale parameter σ at different heights are fitted using exponential functions, while the shape parameter k is obtained through interpolation at various heights.

3. RELIABILITY ANALYSIS OF COASTAL STRUCTURES

3.1 Long-span bridges

Figure 1(a) illustrates the evolution of the probability density distribution of the buffeting response with respect to the mean wind speed of Xihoumen Bridge, represented here by the mid-span RMS acceleration. The predicted probabilistic bounds almost fully encompass the measured scatter of the typhoon-induced response. Theoretically, all measurement data should fall within the high-probability prediction region (the yellow sphere). Figure 1(b) shows the exceeding probability of 10-min peak vertical displacement in mixed climate, which can be further used in loss analysis and performance-based wind design. With the increase in peak displacement threshold, the exceeding probability first diminishes violently and then decreases slowly.

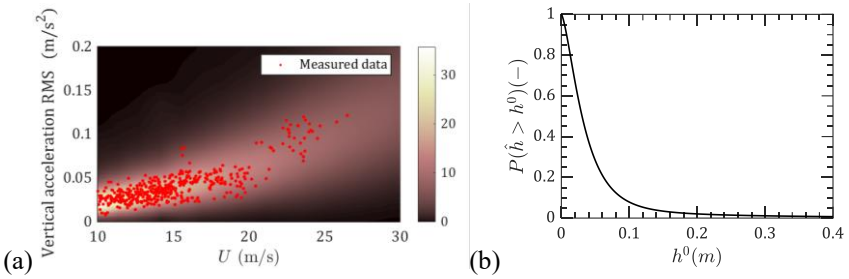

Figure 1: Vertical acceleration RMS: (a) Modeled and measured data; (b) Exceeding probability of peak responses

3.2 Wind Turbine

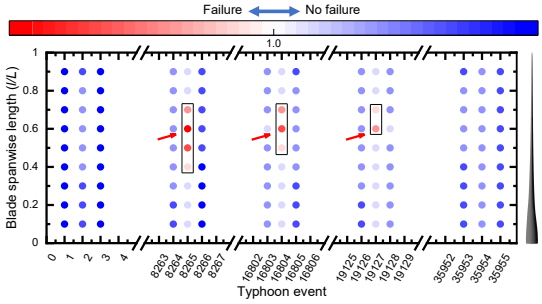

Figure 2. Safety factor of the blade

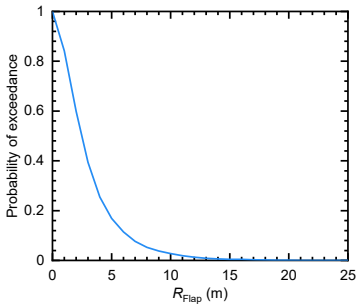

Figure 3. Exceeding probability

Figure 2 show the risk situations of the DTU 10MW wind blade, with each column representing the distribution of safety factors subjected to each typhoon event. It can be observed that under typhoon conditions, the safety factor at the mid-span of the blade is less than 1, indicating that the load exceeds resistance, implying a potential for structural damage. Structural failure is considered to occur when the local load demand at any blade cross-section exceeds its corresponding resistance. The structural reliability indices recommended by ASCE, which are applicable to the typhoon conditions. Because wind-turbine damage under typhoon winds is typically sudden and can lead to substantial economic losses, it is categorized as either sudden or progressive failure. Based on the annual failure probability, the estimated blade failure probability (8.0×10^{-5}) exceeds the ASCE target values. This indicates that, for the selected TC-prone site, the structural safety design of the wind turbine should be further enhanced to withstand extreme typhoon hazards. Figure 3 presents the exceedance probability of blade-tip

deflection, As the peak displacement threshold increases, the exceedance probability drops rapidly and then decreases more gradually.

3.3 Transmission Tower

The selected transmission tower is a self-supporting double-circuit drum-type structure with a total height of 43.6 m and a base height of 27.0 m. The static condensation method is employed to facilitate a significant model order reduction for the transmission tower. The procedure condensed the system from 3,168 to 168 degrees of freedom, thereby enabling a substantial increase in computational efficiency alongside maintained high fidelity, shown in Figure 4. Under a 10,000-year return period typhoon load case, the dynamic response of the reduced-order model is investigated. The frequency-domain modal superposition analysis is conducted to obtain the top displacement time history, based on which the exceeding probability of the peak displacement is evaluated. Figure 5 shows the exceeding probability of the peak response, where the peak responses corresponding to exceeding probabilities of 0.05 and 0.01 are 0.262 m and 0.641 m, respectively.

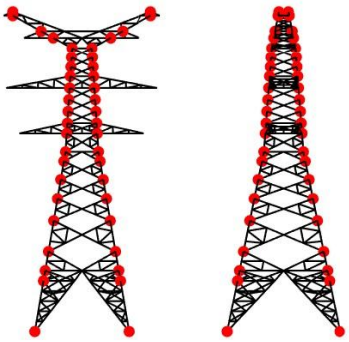

Figure 4. Transmission tower

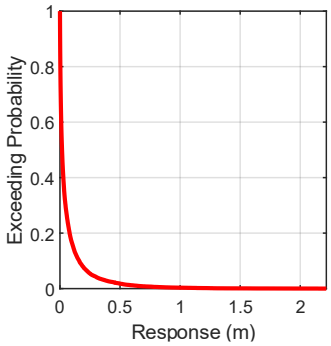

Figure 5. Exceeding probability

ACKNOWLEDGEMENTS

The authors gratefully acknowledge the National Natural Science Foundation of China (52508578), Young Elite Scientists Sponsorship Program by CAST (2023QNRC001), Natural Science Foundation of Shanghai (25ZR1402494).

REFERENCES

Fang G. S., Zhao L., Cao S. Y., Ge Y. J., Pang W., 2018. A novel analytical model for wind field simulation under typhoon boundary layer considering multi-field parameters correlation, Journal of Wind Engineering and Industrial Aerodynamics, 175: 77-89.

Fang G. S., Pang W., Zhao L., Rawal P., Cao S. Y., Ge Y. J., 2021a. Toward a refined estimation of typhoon wind hazards: parametric modeling and upstream terrain effects. Journal of Wind Engineering and Industrial Aerodynamics, 209: 104460.

Fang G. S., Pang W., Zhao L., Cui W., Zhu L. D., Cao S. Y., Ge Y. J., 2021b. Extreme typhoon wind speed mapping for coastal region of China: a geographically-weighted-regression-based circular subregion algorithm. Journal of Structural Engineering, 147(10): 04021146.

Hu, L., Xu, Y.L., Huang, W.F., 2013. Typhoon-induced non-stationary buffeting response of long-span bridges in complex terrain. Engineering Structures 57, 406-415.

Liu Z. H., Fang G. S., Hu X. N., Xu K., Zhao L., Ge Y. J., 2022. Stochastic power spectra models for typhoon and non-typhoon winds: a data-driven algorithm. Journal of Wind Engineering and Industrial Aerodynamics, 231: 105214.

Liu Z. H., Fang G. S., Zhao L., Ge Y. J., 2023. Uncertainty propagation of turbulence parameters for typhoon and non-typhoon winds in buffeting analysis of long-span bridges. Engineering Structures, 291: 116491.